2011

# Ultrafast REMPI in benzene and the monohalobenzenes without the focal volume effect

Timothy D. Scarborough
*University of Nebraska-Lincoln*, tim.d.scarborough@gmail.com

James Strohaber
*Texas A & M University - College Station*, jstroha1@gmail.com

David B. Foote
*University of Nebraska-Lincoln*

Collin J. McAcy
*University of Nebraska-Lincoln*, s-cmcacy1@unl.edu

Cornelis J. Uiterwaal
*University of Nebraska-Lincoln*, cuiterwaal2@unl.edu

# PCCP

**PAPER**

# Ultrafast REMPI in benzene and the monohalobenzenes without the focal volume effect

**Timothy D. Scarborough,**[*a] **James Strohaber,**[b] **David B. Foote,**[a] **Collin J. McAcy**[a] **and Cornelis J. G. J. Uiterwaal**[a]

We report on the photoionization and photofragmentation of benzene ($C_6H_6$) and of the monohalobenzenes $C_6H_5$–X (X = F, Cl, Br, I) under intense-field, single-molecule conditions. We focus 50-fs, 804-nm pulses from a Ti:sapphire laser source, and record ion mass spectra as a function of intensity in the range $\sim 10^{13}$ W/cm$^2$ to $\sim 10^{15}$ W/cm$^2$. We count ions that were created in the central, most intense part of the focal area; ions from other regions are rejected. For all targets, stable parent ions ($C_6H_5X^+$) are observed. Our data is consistent with resonance-enhanced multiphoton ionization (REMPI) involving the neutral $^1\pi\pi^*$ excited state (primarily a phenyl excitation): all of our plots of parent ion yield versus intensity display a kink when this excitation saturates. From the intensity dependence of the ion yield we infer that both the HOMO and the HOMO−1 contribute to ionization in $C_6H_5F$ and $C_6H_5Cl$. The proportion of phenyl ($C_6H_5$) fragments in the mass spectra increases in the order X = F, Cl, Br, I. We ascribe these substituent-dependent observations to the different lifetimes of the $C_6H_5X$ $^1\pi\pi^*$ states. In X = I the heavy-atom effect leads to ultrafast intersystem crossing to a dissociative $^3n\sigma^*$ state. This breaks the C–I bond in an early stage of the ultrashort pulse, which explains the abundance of fragments that we find in the iodobenzene mass spectrum. For the lighter X = F, Cl, and Br this dissociation is much slower, which explains the lesser degree of fragmentation observed for these three molecules.

## Introduction

The desire to control chemical reactions[1,2] and to improve the generation of short-wavelength radiation[3] are among the main forces driving the continuing widespread interest in molecular intense-field dynamics.[4] For instance, current methods to produce attosecond light pulses[5] are based on the widely accepted rescattering model.[6] An important aspect of the present work is parent ion formation (M → M$^+$). Ultrafast pulses typically produce significant amounts of parent ions, more than nanosecond or picosecond pulses. The high optical pumping rate of ultrafast pulses efficiently competes with neutral dissociation rates, even if the latter are on the femtosecond time scale. This "impulsive ionization"[7] facilitates the mass-spectroscopic identification of trace analysis. Research on the stability of ionized aromatics is also relevant for modeling of the interstellar medium. If these ions exist, they may contribute considerably to interstellar UV opacity by absorbing UV radiation, converting

electronic energy into vibrational energy, and emitting strong IR features.[8,9]

The resources needed for fully *ab initio* computational studies of molecular photodynamics in intense fields are far beyond reach.[10] Practicable quantum-chemical computational simulations rely on drastic simplifications. For instance, Karlsson *et al.*[11] recently reported simulations for substituted benzenes in which the whole aromatic electron system is assumed to be largely unaffected by photoexcitation to its lower excited states. Such approximations require experimental validation.
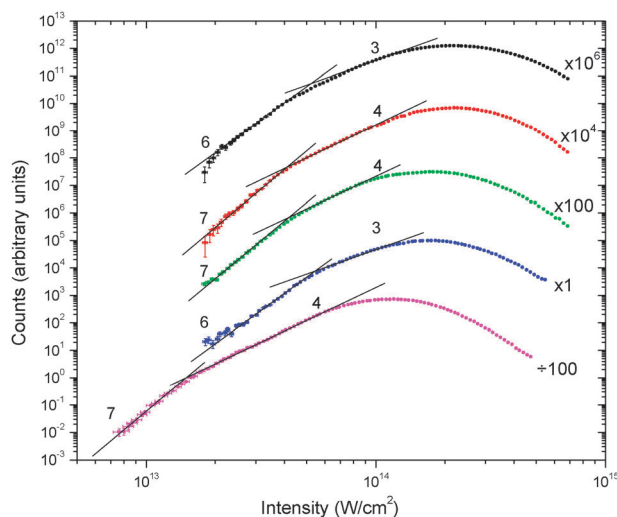
In our current experimental work we investigate the photodynamics of the monohalobenzenes $C_6H_5X$ (X = F, Cl, Br, I). Our goal is to study the photodynamics of systematic series of analogous molecules which differ from each other in a single structural parameter, here the atomic halogen. This approach allows us to study the effects of the atomic substituent on molecular intense-field photodynamics. Structural parameters can only be varied in discrete steps, in the present case simply because there are only four halogen atoms (ignoring the short-living radioactive astatine atom, At). We selected monosubstituted aromatic molecules because their ionization is facilitated by a resonance in the phenyl group, and because of their relevance as pointed out above. In addition, the series

[a] *Department of Physics and Astronomy, University of Nebraska – Lincoln, Lincoln, NE, USA. E-mail: tim.scarborough@huskers.unl.edu*
[b] *Department of Physics and Astronomy, Texas A&M University, College Station, TX, USA*

This journal is © the Owner Societies 2011

*Phys. Chem. Chem. Phys.*, 2011, **13**, 13783–13790 | 13783

of monohalobenzenes is easily expanded into the wider group of substituted benzenes. These have the general structural formula $C_6H_5$–R, where R is a substituent functional group such as the nitro group –$NO_2$ or the methyl group –$CH_3$. Such functional groups often determine the characteristic role of a substituted molecule in an application, which makes them worth investigating.

We present the parent ion yields of benzene ($C_6H_6^+$), fluorobenzene ($C_6H_5F^+$), chlorobenzene ($C_6H_5Cl^+$), bromobenzene ($C_6H_5Br^+$), and iodobenzene ($C_6H_5I^+$) as a function of pulse intensity, under single-molecule conditions. We focus ultrashort (50 fs, 804 nm) pulses into the target vapor and record ion yields as a function of pulse energy from a micrometer-sized interaction volume only, inside which the intensity varies by less than 1/14th of a decade on a logarithmic intensity axis. This small variation, without the need for deconvolution,[12–16] eliminates focal averaging. Further details on the method used to suppress signal averaging can be found in the Appendix. By suppressing signal averaging[17] over the wide range of intensities found in the focal spot (the volume effect), we observe features in the ion yields of aromatic molecules that are fingerprints of molecular resonance-enhanced multiphoton ionization (REMPI).[18] Ionizing through an intermediate excited state allows us to study not only the ionization mechanisms, but the properties of the excited states themselves. These excited states are more greatly affected by the Stark effect,[19] increasing the ability of the laser field to influence subsequent photochemical processes.[20]

**Table 1** **Mathematically fitted results.** Fitted slopes were determined by plotting $^{10}\log$(yield) *vs.* $^{10}\log$(intensity) and fitting to linear trends weighted by the error bars over the relevant regions. A description of the fitting routine can be found in Appendix 1. Ionization potentials are included for comparison

| Species | IP (eV) | Low intensity slope | High intensity slope |
|---|---|---|---|
| Benzene | 9.24 | $6.27 \pm 0.10$ | $\sim 3.5 \pm 0.1$ |
| PhF | 9.20 | $7.03 \pm 0.12$ | $4.00 \pm 0.02$ |
| PhCl | 9.07 | $6.80 \pm 0.10$ | $4.02 \pm 0.04$ |
| PhBr | 9.00 | $5.93 \pm 0.09$ | $3.03 \pm 0.06$ |
| PhI | 8.85 | $6.71 \pm 0.21$ | $3.97 \pm 0.02$ |

Our measured ion yields are presented in Fig. 1, in which the logarithm of the ion yield $Y$ is plotted against the logarithm of the pulse intensity $I$. This double-logarithmic representation is customary and convenient in studies of intense-field ionization, because ion yields from multiphoton processes, which rise as $Y \propto I^m$, where $m$ is the number of photons involved, appear as straight lines with slope $m$. Based on our estimates of the Keldysh parameter,[21] MPI is expected; this is supported by the existence of several such straight lines with integer slope in our experimental data. Fitted values for the slopes are presented in Table 1. We find that each target molecule has two regions of intensities with constant integer slope, a signature of REMPI. In this process a resonant transition to an excited molecular state becomes saturated such that a smaller number of photons is capable of ionizing from this immediately-populated excited state. This excited state is the $^1\pi\pi^*$ ($1\,^1B_2$) state which has been well-documented in the halobenzenes through nanosecond UV (1 + 1) REMPI experiments around 266 nm.[22–24] The monohalobenzenes all follow ($m + n$) REMPI patterns. At the highest intensities used, the parent ion yields of all five species rapidly decrease as other processes become dominant, such as multiple ionization and fragmentation.

## Results and discussion

The curve for benzene most closely indicates a slope-six to slope-three kink, representative of a (3 + 3) REMPI process. However, both slopes rise slightly more quickly than this (see Table 1). Because the six-photon range of our 804 nm photons is 9.25 eV $\pm$ 0.06 eV (with the uncertainty due to the bandwidth of the femtosecond pulses), six photons are not always enough to exceed the ionization potential, 9.24 eV, and so we expect some mixing of six- and seven-photon processes. Similarly, the transition from the excited to ionic state in benzene is barely within range of three, resulting in some mixing between three- and four-photon processes. The six-photon result matches previous results carried out at 800 nm.[25]

In fluorobenzene and chlorobenzene we observe a seven-photon to four-photon absorption, indicative of (3 + 4) REMPI. This seems counterintuitive, as the ionization potential of both molecules (9.20 eV and 9.07 eV for fluorobenzene and chlorobenzene, respectively) are within the energy of six photons. Channel closing was investigated as a possible explanation, but was determined to be unsuitable, as discussed further below.



**Fig. 1** **Parent ion yields of benzene and the monohalobenzenes.** Molecular parent ion yields of benzene (black), fluorobenzene (red), chlorobenzene (green), bromobenzene (blue), and iodobenzene (pink) as a function of intensity, measured with 804 nm, 50 fs pulses. Data has been normalized for consistency in pressure and collection time, and has been shifted vertically by two orders of magnitude per dataset to allow viewing on the same graph. Errors in the count rate are based on counting statistics, while errors in intensity are estimated from experimental uncertainties in power measurement and laser stability. Thin black lines, marked with the log-log slope (and thus the number of photons in the process) are meant to guide the eye, and represent our determination of the most accurate integer slope. Mathematically fitted slope values can be found in Table 1.

However, it has been put forward that in substituted benzenes the highest occupied molecular orbital (HOMO) and the HOMO−1 may contribute significantly to ionization.[26] For fluorobenzene and chlorobenzene, there is a difference in energy of the HOMO and HOMO−1 of approximately 0.6 eV,[27] which is enough to account for (3 + 4) REMPI if the HOMO−1 transition is more strongly on resonance with an excited state, which seems to be the case here. It is notable that the HOMO−1 plays a role in the halobenzenes but not in benzene; in the higher symmetry of benzene (point group $D_{6h}$), the two highest occupied MOs are degenerate ($e_{1g}$ character), and their contributions to ionization cannot be considered independently. The addition of a halogen substituent lowers the molecular symmetry in the halobenzenes to point group $C_{2v}$. This lifts the degeneracy of the HOMO and HOMO−1; in PhCl (Ph = phenyl group), for instance, these MOs have character $b_1$ and $a_2$, respectively.[28] A degeneracy in the $^1\pi\pi^*$ excited state is similarly lifted, resulting in another possible excitation pathway.

Bromobenzene has an even lower ionization potential (9.00 eV), which allows for a six-photon process to dominate the ionization. As the resonant three-photon transition (ground state to $^1\pi\pi^*$) saturates, three-photon ionization takes over. Here ionization from the HOMO−1, which would require seven photons, seems to be insignificant. The heavier halogen substituents induce a larger splitting between the

energies of the HOMO and HOMO−1, which seems to push the HOMO−1 farther from a resonant transition.

Of particular interest is iodobenzene, where we observe a seven- to four-photon kink. It is generally accepted that 266-nm (within the same energy spread of three 804-nm photons) excitation of PhI excites the HOMO into a bound $^1\pi\pi^*$ state,[29–34] so we expect this transition to be strongly resonant. This singlet state rapidly predissociates to a repulsive $^3n\sigma^*$ triplet state, which leads to bond cleavage in the neutral molecule: PhX* → Ph + X; similar nonradiative decay has been observed in heteroaromatic molecules.[35,36] Unlike the other halobenzenes, which have PhX* $^1\pi\pi^*$ lifetimes ranging from hundreds of picoseconds to several nanoseconds, the unperturbed lifetime of the PhI* $^1\pi\pi^*$ state is between 20 fs and 700 fs.[31,37–40] This ultrafast intersystem crossing in iodobenzene is due to the strong spin–orbit coupling induced by the iodine atom. For the lighter halogen substituents this coupling is smaller (internal heavy atom effect)[40] and intersystem crossing is unlikely. In our mass spectra for iodobenzene we observe not only an abundance of Ph$^+$ and I$^+$, but also ionic states of the iodine atom through I$^{8+}$, which indicates that an absorption, a predissociative intersystem crossing, and a nascent dissociation occur quickly enough to leave time to ionize the now-independent atom up to eight times (PhI → PhI*($^1\pi\pi^*$) → PhI*($^3n\sigma^*$) → Ph$^+$ + I$^{N+}$) before the end of the 50-fs laser pulse. As expected for ultrafast intersystem
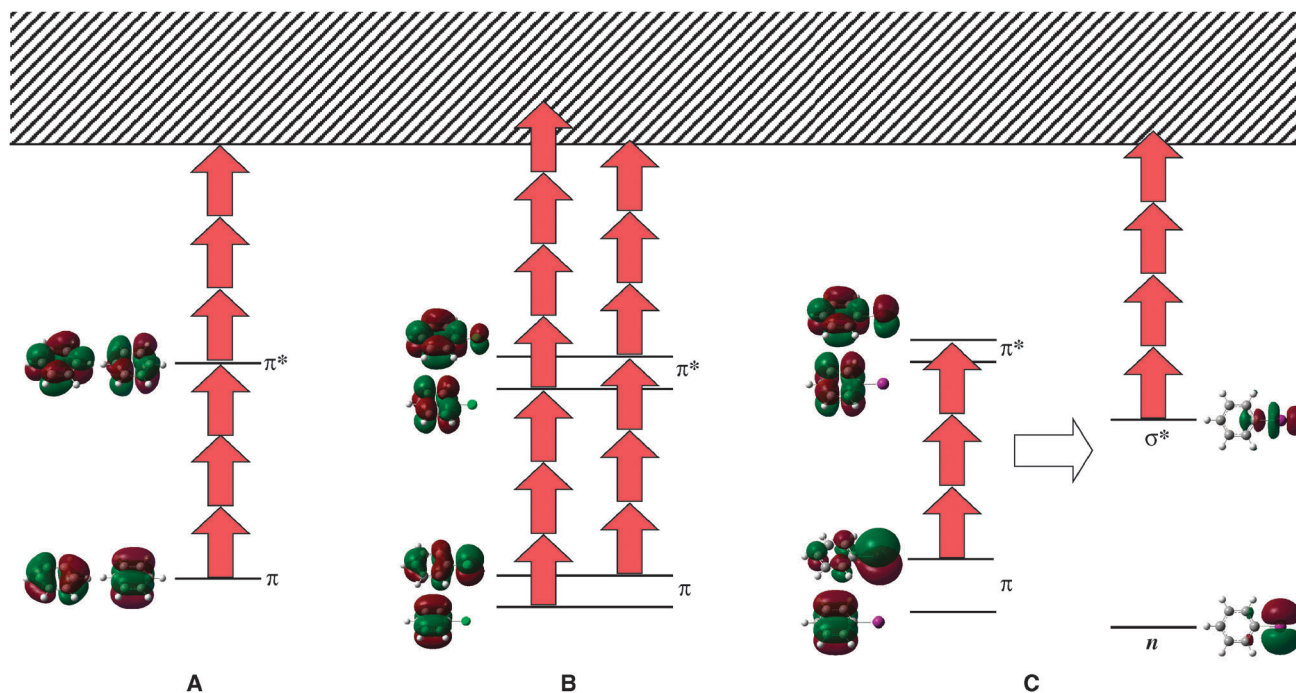


**Fig. 2** Energy level diagram of observed processes in benzene and the monohalobenzenes (energies not to scale). (A) Sketch of (3 + 3) REMPI observed in benzene. Photons are shown as red arrows, the ionization continuum is shown as a checkered area, and the relevant molecular orbitals are shown next to the energy levels. (B) Sketch of REMPI processes involving the HOMO and HOMO−1. In the monohalobenzenes the degenerate benzene $\pi$ ($e_{1g}$) and $\pi^*$ ($e_{1g}$) levels are split. In this panel **B**, the left column of arrows shows (3 + 4) REMPI as seen in fluorobenzene and chlorobenzene dominated by the HOMO−1, and the right column shows (3 + 3) REMPI as seen in bromobenzene where the HOMO−1 does not contribute. (C) Sketch of 3-photon excitation from the HOMO, ultrafast intersystem crossing to a dissociative triplet state, and 4-photon ionization as seen in iodobenzene. The intersystem crossing involves an electronic orbital rearrangement, which ends with the HOMO filled and unpaired electrons in both the $n$ and $\sigma^*$ states.
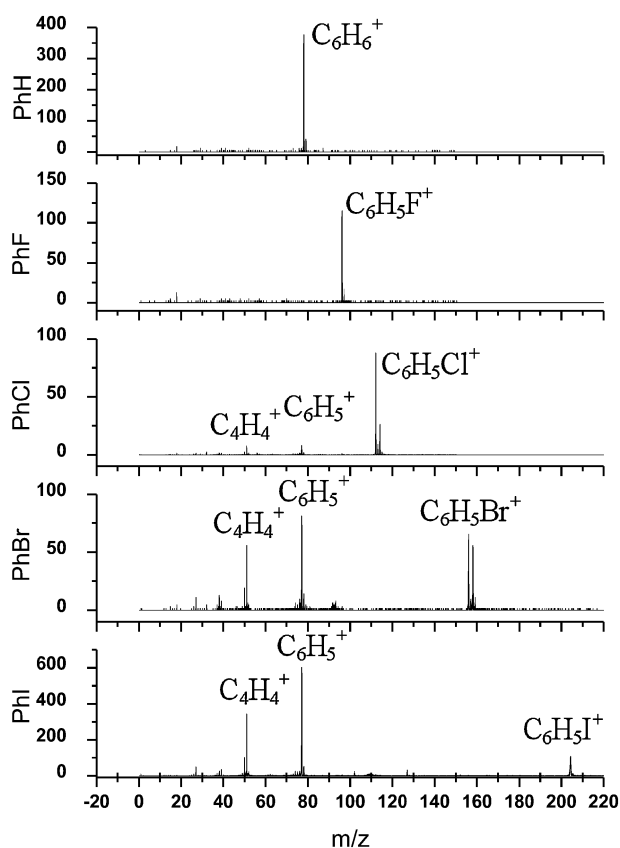
**Fig. 3  Raw mass spectra.** The mass spectra for each halobenzene, shown here for intensity $4 \times 10^{13}$ W/cm$^2$, indicate the increased presence of the phenyl ion ($C_6H_5^+$). This signifies the importance of the internal heavy-atom effect in the dissociation of the halobenzenes.

crossing in PhI we observe fragments in its mass spectrum even for the lowest intensities, while fragments of the other halobenzenes are absent (or appear in trace amounts). Further, the energy difference of the HOMO and HOMO−1 in iodobenzene is $\approx 0.73$ eV (nearly half the energy of a photon),[27] so given that the HOMO is strongly resonant, the contribution of the HOMO−1 is unlikely to contribute to resonant excitation. We thus disregard the role of the HOMO−1 here. This makes the observed slope of four intriguing. Ionizing from the $^1\pi\pi^*$ state would not yield a four-photon process; it is well within the range of three photons. However, ionization from the $^3n\sigma^*$ state during the dissociation explains the four-photon process. Thus, we determine that the slope of four is representative of a three-photon excitation to the singlet $^1\pi\pi^*$ state followed by a nearly immediate intersystem crossing to the dissociative triplet $^3n\sigma^*$ state, which then requires four photons to ionize before it can completely dissociate,[22,29] as shown in Fig. 2c. As a result, we find a four-photon process for more than half a decade in intensity.

The importance of the intersystem crossing is clear in the mass spectra, as shown in Fig. 3. The internal heavy atom effect increases the likelihood of the dissociation to the phenyl radical and atomic halogen, and perhaps unsurprisingly, we observe increasing amounts of the ionized phenyl with heavier substituents. What may be surprising, however, is that the phenyl ion peak overtakes the parent ion peak in the
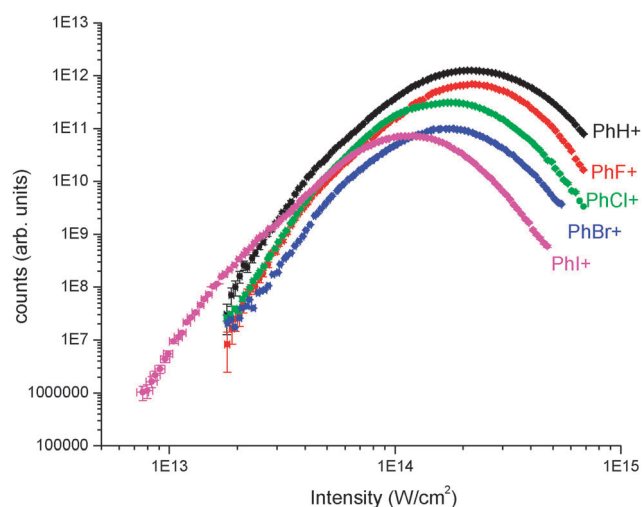


**Fig. 4  Ionization suppression.** Molecular parent ion yields of benzene (black), fluorobenzene (red), chlorobenzene (green), bromobenzene (blue), and iodobenzene (pink) as seen in Fig. 1 without scaling for easier viewing. In this representation, the suppression of the ion yields due to the increased number and likelihood of higher-order channels (multiple ionization, dissociation, *etc.*) becomes increasingly evident.

iodobenzene spectrum. The apparent peak-to-peak ratio is somewhat misleading; the bin width is constant in time, and since the time of flight scales as $(m/q)^{1/2}$, at higher masses the peaks spread out over more bins, giving the appearance of a smaller peak height.

Nevertheless, throughout the majority of the intensity range studied, the phenyl ion yield is between one and three times greater than the parent ion yield in iodobenzene. Although dissociation is the leading process (particularly at higher intensities), rate model calculations suggest that the log–log slopes of seven and four remain unaffected under the given conditions.

## Parent ion yield suppression

In addition to the dynamics, we must examine the more general effects of the substituents on the ion yields. One expects that as dissociation and fragmentation channels become more prevalent, the yield will saturate at a lower intensity. Further, one expects that the probability of creating a singly-charged ion is lowered due to the increased number of loss channels; benzene has fewer (and less likely) dissociation channels than the halobenzenes.

**Table 2  Saturation intensity and ionization suppression.** The intensity at which the parent ion yield reaches its maximum, known as the saturation intensity, decreases notably with increasing halogen size. Additionally, the relative parent ion yield at the saturation intensity decreases dramatically compared to benzene. Ionization potentials are included for comparison

| Species | $I_{sat}$ ($10^{14}$ W/cm$^2$) | Relative counts at $I_{sat}$ | IP (eV) |
|---|---|---|---|
| $C_6H_6$ | 2.18 | 1 | 9.24 |
| $C_6H_5F$ | 2.19 | 0.555 | 9.20 |
| $C_6H_5Cl$ | 1.77 | 0.249 | 9.07 |
| $C_6H_5Br$ | 1.73 | 0.079 | 9.00 |
| $C_6H_5I$ | 1.15 | 0.057 | 8.85 |
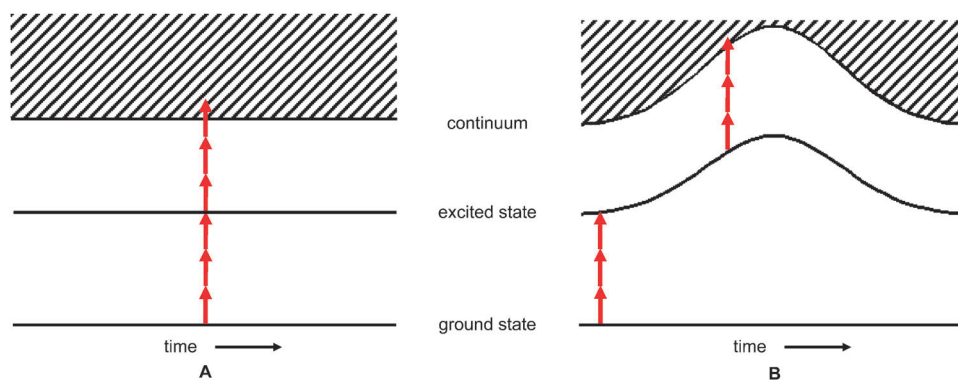
**Fig. 5  Effects of the ponderomotive shift.** At low intensities (A), the ponderomotive energy shifts are small. At higher intensities (B) when the ponderomotive shift becomes significant, the now-saturated resonant excitation occurs very quickly on the rising edge of the pulse. Unlike the ground state, the excited states undergo an energy shift comparable to the continuum before absorbing another three photons (red arrows) to ionize. This ultimately renders the shift irrelevant.

This is indeed what we find. The authors wish to address the point, once again, that saturation intensities were previously inferred from the limiting slope of the yield *vs.* log(*I*) plots when full three-dimensional spatial resolution was not available;[41] here values are not inferred but measured directly.

As detailed in Table 2, the dependence of saturation intensity on the likelihood of fragmentation is not entirely simple; bromobenzene fragments much more easily than chlorobenzene, yet they have very similar saturation intensities. There also seems to be a strong correlation of saturation intensity with the ionization potential of the molecule, with benzene and fluorobenzene being very similar, chlorobenzene and bromobenzene being very similar, and iodobenzene being much smaller than the rest. The maximum ion yield at the saturation intensity of each halobenzene is considerably smaller than that of benzene, which is not surprising due to the increased number of dissociation channels.

**Channel closing ruled out as an explanation of slopes that do not match ionization potentials**

In the results for fluorobenzene, chlorobenzene and iodobenzene, we see initial rising slopes of seven even though, based on their known ionization potentials, we expect six photons to be sufficient to ionize. One possible explanation that was explored was channel closing, a phenomenon in which the intense field induces a ponderomotive (AC Stark) shift of the energy levels until the *n*-photon channel is no longer accessible, and ionization can only be achieved by an (*n* + 1)-photon process. This seems reasonable given that the ponderomotive energy at $\sim 10^{13}$ W/cm$^2$ is about 0.6 eV.

Based purely on ionization potential, channel closing should be stronger in benzene than in fluoro- and chlorobenzene, but we see the opposite. One could conclude that the molecular symmetry ($D_{6h}$ for benzene and $C_{2v}$ for the halobenzenes) could affect how the energy levels couple to the field, but bromobenzene seems to be unaffected; if the six-photon channel is open in bromobenzene, it would also be open in iodobenzene, where we also see a dominant seven-photon process. We conclude that even if channel closing sufficiently explains the seven-photon processes in fluorobenzene and chlorobenzene, it does not explain the seven-photon process in iodobenzene.

Perhaps most importantly, we determine that channel closing, even if it explained the initial slopes of seven, would be inconsistent with the subsequent slopes of four. Because the ionization occurs from an excited state, we still expect a slope of three after the resonance saturates. As illustrated in Fig. 5, the resonant excitation occurs when the ponderomotive energy is small; at low intensities this can occur throughout the pulse, but at high intensities it occurs very quickly on the rising edge of the pulse. After excitation, the energy shift of the excited states is expected to be comparable to the energy shift of the continuum,[19] making the shift irrelevant to ionization. This is further enhanced due to the aromaticity of the molecules and the resulting delocalization of the orbitals in question,[42] as the delocalized electrons are essentially free to move with the field within their bound state. We thus conclude that channel closing is not consistent with our results.

## Conclusions

A resonant transition to a $^1\pi\pi^*$ excited state is relevant for all five aromatic molecules we have investigated. The phenyl group inherits this resonance from the benzene aromatic system; in more complex substituted benzenes the perturbation of this aromatic orbital system will depend on the nature and number of functional groups of various kinds. For instance, the behavior in the photochemical stability of certain DNA bases can be attributed to such excited states.[43]

The dominating feature in regard to the comparative ionization suppression of the halobenzenes seems to be the increasing strength of the spin–orbit coupling across the series F < Cl < Br < I. The spin–orbit coupling causes an increased likelihood of dissociation and, in the case of iodobenzene, interrupts the standard two-stage REMPI process with a singlet–triplet intersystem crossing.

Modern techniques to create attosecond pulses are rooted in electron rescattering in intense field ionization.[6] In light of

the present work, rescattering and other processes[44] that rely on intense-field ionization must account for simultaneous (or competing) ionization from the molecular HOMO and the HOMO−1 orbitals (or more MOs, which also may be degenerate), and the interpretation of the produced attosecond pulses or molecular images must be done with prudence.

## Appendix: Materials and methods

### Eliminating focal averaging

We recorded ions using a reflectron-type time-of-flight (TOF) ion mass spectrometer from a micrometer-sized interaction volume only, inside which the intensity varies by less than 1/14th of a decade on a logarithmic axis. This small variation, without the need for deconvolution, eliminates focal averaging. Mass spectrometers are often tuned such that ions from all positions in the focus are detected at the same TOF; our system, however, is deliberately tuned to create a linear dependence of the TOF on the initial position of the ions in the focus. As a result, the spatial distribution in the focus is mapped directly onto the TOF spectrum. A full description of this approach is found in ref. 17. We emphasize that the structures we observe (straight lines, kinks, and drops) would have escaped observation when, following common practice, ions had been recorded from the entire focal region, an approach termed 'full view' (FV).[12] To make this point, it would have been instructive to show the FV version of our PhX$^+$ (Ph = phenyl group, X = halogen) data; unfortunately, no such curves have been reported in the literature. However, benzene has been studied extensively, for instance by Talebpour et al.;[25] therefore, we measured benzene as well. In Fig. 6 our data (red squares) is shown along with the FV data of ref. 25 (black circles). For the purpose of direct comparison, our data is shifted in intensity by a constant factor to compensate for differences in intensity calibrations between different groups' data. Such a shift does not distort the results other than to displace the saturation intensity. Based on our current benzene data we have simulated (blue curve) the yields we would have found if we had used the FV approach; this simulation agrees with the experimental FV data, even overlapping their theoretical curve (dashed curve). The data of ref. 25, like any using a FV approach, suffers from a $Y \propto I^{3/2}$ dependence (slope 3/2) for the highest intensities. This is a conspicuous feature of all FV curves: an artifact unrelated to the actual underlying molecular dynamics.[13] At the highest intensities, the FV slope-3/2 data is about three orders of magnitude different from our true data, a dramatic discrepancy arising from the different acceptance volume sizes. The single property the FV curves inherit from the true ones is their slope for lowest intensities; we have overlapped the FV curves with our data to demonstrate this limited agreement.

Because the FV approach has prevented previous works from identifying the presently observed kinks, we emphasize the importance of excluding the possibility that the kinks in the PhX$^+$ yields are not an artifact of our approach. To do so, we also investigated the ionization of atomic xenon, in which we expect no such resonant features. We observe that the Xe$^+$ yield does not feature a kink; it rises in agreement
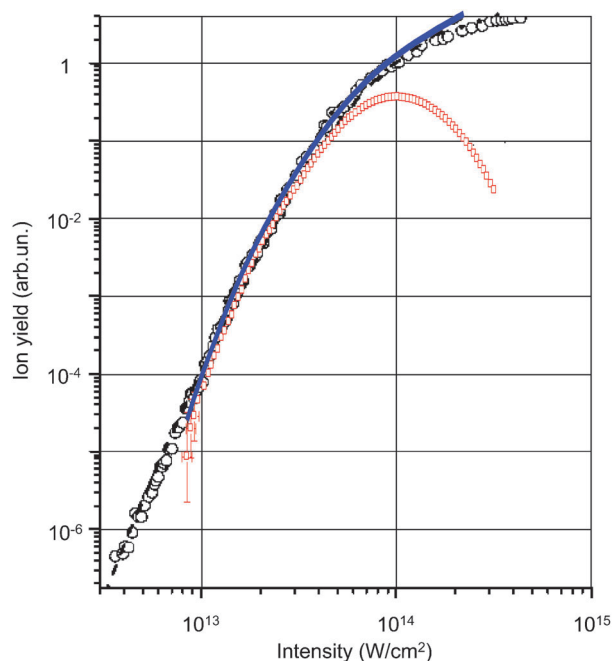


Fig. 6 **The effect of eliminating focal averaging.** Red open squares: our $C_6H_6^+$ yield as a function of pulse intensity. For comparison we show the results of ref. 25, where ions were collected from a large region of the focus (full-view, FV): experimental yield (black open circles) and theoretical prediction (black dashed line). For the purpose of direct comparison, our data is shifted in intensity by a constant factor to compensate for differences in intensity calibrations between the data. The structures in our measured ion yields at $\sim 2 \times 10^{13}$ W/cm$^2$ are washed out in ref. 25 due to integration over the focal volume. Additionally, for intensities beyond $\sim 10^{14}$ W/cm$^2$ our ion yield decreases due to competing processes, such as multiple ionization and fragmentation. By contrast, the FV $C_6H_6^+$ yield keeps increasing with a slope of 3/2, an artifact due to the growing size of the focus. We simulated (blue curve) the FV data by convoluting our own data into a much larger ($100 \times 100 \times 2000$ μm) acceptance volume. This focal integration washes out our structures.

with FV results of other groups.[45,46] We conclude our kinks are genuine.

### Determining mathematically-fitted slope values

Plotting the logarithm of the yield against the logarithm of the intensity, as mentioned previously, results in a linear slope equal to the number of photons in the process. In each case, as seen in Fig. 7, the range over which a slope was fitted was determined by finding the limits where, by including more data points of higher or lower intensity, the slope no longer remained consistent, whereas removing points did not significantly change the slope. This can be done objectively in all cases except benzene where, as discussed in the main text, we expect some mixing of three- and four-photon processes. As a result, the inclusion or rejection of single points does not result in a consistent slope over a large range at the higher intensities in benzene, and this slope is thus open to some subjectivity.

### Experimental parameters

We used 804-nm ($\hbar\omega = 1.54$ eV), 50-fs pulses produced by a Ti:sapphire laser system based on chirped-pulse amplification.

These pulses were focused into a target vacuum chamber at stagnation pressures of $\sim 5 \times 10^{-7}$ mbar, with this pressure
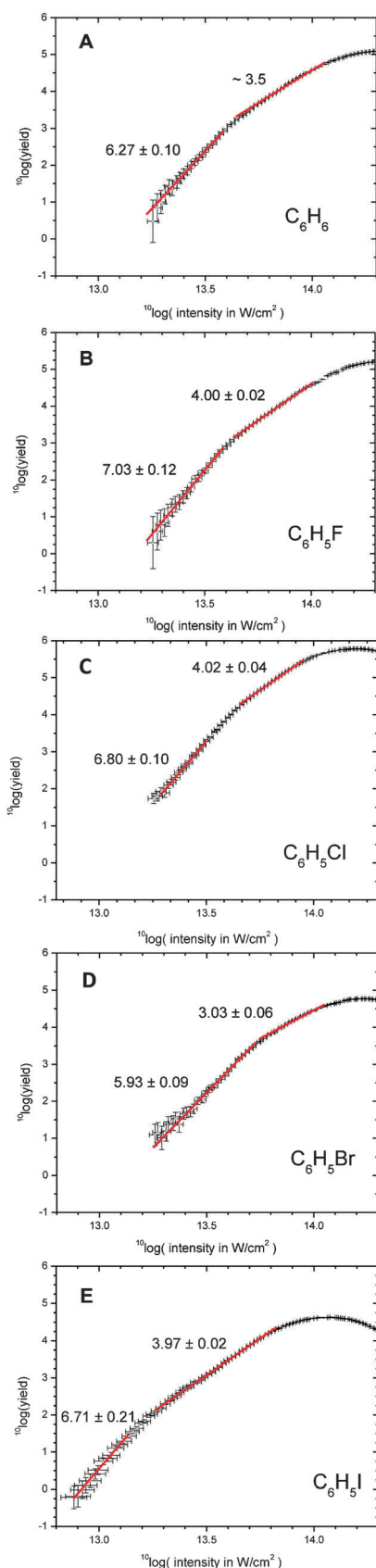


chosen to maximize the count rate while avoiding high-pressure distortions in the data. The resulting Gaussian laser focus, as measured with beam imaging software, was found to be 35 μm in FWHM. Intensities were calibrated by mixing benzene and xenon in the chamber and adjusting our calculated intensities to the well-documented saturation intensity of xenon.[45,46] Rotating a half-wave plate in the laser's compressor allowed adjustable attenuation of the beam ranging from $\sim 1 \times 10^{13}$ W/cm$^2$ to $\sim 4 \times 10^{14}$ W/cm$^2$. This range of intensities was adequate for identifying the relevant processes in all molecules considered except iodobenzene; to achieve low enough intensities for iodobenzene, a 50% transmission neutral density filter was inserted in the beam path, and was used only for intensities less than $1 \times 10^{13}$ W/cm$^2$. Frequency resolved optical gating[47] measurements showed no significant changes in pulse quality or duration as a result of the neutral density filter.

Ions were detected with a double microchannel plate, the signal of which we fed into a counting card controlled by a PC. The spectrometer was tuned to map the spatial ion densities created by the laser pulses in the focus onto the TOF spectrum; by setting a region of interest in the TOF spectrum we then count ions created in a micrometer-sized, limited detection volume only. Ion counts from outside the detection volume are simply discarded. Inside this detection volume the intensity is almost constant. Further details of the three-dimensional spatial ion resolution can be found in ref. 17.

For the present measurements we adjusted the dimensions of the detection volume to 500 μm (along the laser propagation direction) × 15 μm × 15 μm (along the two transverse directions); we estimate that more than half of the detection volume is between 85–100% of the maximum intensity, and none of the volume is below 50%, which limits errors to $\sim$1/14th of a decade of a logarithmic intensity axis. This estimate includes possible vibrations and laser pointing variations of up to $\pm$ 4 micrometers standard deviation. The intrinsic fluctuations in the laser pulse energy were less than 8%. All target chemicals were obtained from Aldrich, with purity 99.5% or better (99.0% for iodobenzene), and used as purchased.

## Acknowledgements

**Fig. 7 Mathematically-fitted slopes.** Plotting the logarithm of the yield against the logarithm of the intensity, seen for benzene (A), fluorobenzene (B), chlorobenzene (C), bromobenzene (D) and iodobenzene (E), results in a linear slope equal to the number of photons in the process. Linear fits are presented for high- and low-intensity regions.

## Notes and references

1 H. Rabitz, *Science*, 2003, **299**, 525.
2 H. Rabitz, *Science*, 2006, **314**, 264.
3 W. Boutu, S. Haessler, H. Merdji, P. Breger, G. Waters, M. Stankiewicz, L. J. Frasinski, R. Taieb, J. Caillat, A. Maquet, P. Monchicourt, B. Carre and P. Salieres, *Nat. Phys.*, 2008, **4**, 545.
4 I. V. Hertel and W. Radloff, *Rep. Prog. Phys.*, 2006, **69**, 1897.
5 Zenghu Chang, *Fundamentals of Attosecond Optics*, CRC Press, 2011.
6 P. B. Corkum, *Phys. Rev. Lett.*, 1993, **71**, 1994.
7 T. Imasaka, *Chem. Rec.*, 2008, **8**, 23.
8 F. Salama and L. J. Allamandola, *Nature*, 1992, **358**, 42.
9 M. Rosi, C. W. Bauschlicher Jr. and E. L. O. Bakes, *Astrophys. J.*, 2004, **609**, 1192.
10 Methods are beyond reach, however see http://www.physorg.com/news194276894.html. Though impressive, this research required immense and costly resources on a record supercomputer, with software developed and specifically optimized for its architecture. No resources exist to simulate the intense-field photodynamics of larger molecules.
11 D. Karlsson, O. Anders Borg, S. Lunell, J. Davidsson and H. O. Karlssona, *J. Chem. Phys.*, 2008, **128**, 034307.
12 L. Robson, K. W. Ledingham, P. McKenna, T. McCanny, S. Shimizu, J. M. Yang, C. G. Wahlström, R. Lopez-Martens, K. Varju, P. Johnsson and J. Mauritsson, *J. Am. Soc. Mass Spectrom.*, 2005, **16**, 82.
13 S. Speiser and J. Jortner, *Chem. Phys. Lett.*, 1976, **44**, 399.
14 T. R. J. Goodworth, W. A. Bryan, I. D. Williams and W. R. Newell, *J. Phys. B: At., Mol. Opt. Phys.*, 2005, **38**, 3083.
15 M. A. Walker, P. Hansch and L. D. Van Woerkom, *Phys. Rev. A: At., Mol., Opt. Phys.*, 1998, **57**, R701.
16 J. Strohaber, A. A. Kolomenskii and H. A. Schuessler, *Phys. Rev. A: At., Mol., Opt. Phys.*, 2010, **82**, 013403.
17 J. Strohaber and C. J. G. J. Uiterwaal, *Phys. Rev. Lett.*, 2008, **100**, 23002.
18 J. H. Posthumus, *Rep. Prog. Phys.*, 2004, **67**, 623.
19 M. P. de Boer and H. G. Muller, *Phys. Rev. Lett.*, 1992, **68**, 2747.
20 B. J. Sussman, D. Townsend, M. Y. Ivanov and A. Stolow, *Science*, 2006, **314**, 278.
21 L. V. Keldysh, *Sov. Phys. JETP.*, 1965, **20**, 1307 [English translation of (1964) *Zh. Eksp. Teor. Fiz.*, 1964, **47**, 1945].
22 X.-P. Zhang, Z.-R. Wei, W.-B. Lee, T.-J. Chao and K.-C. Lin, *ChemPhysChem*, 2008, **9**, 1721.
23 J. Philis, A. Bolovinos, G. Andritsopoulos, E. Pantos and P. Tsekeris, *J. Phys. B: At. Mol. Phys.*, 1981, **14**, 3621.
24 O. K. Yoon, W. G. Hwang, J. C. Choe and M. S. Kim, *Rapid Commun. Mass Spectrom.*, 1999, **13**, 1515.
25 A. Talebpour, A. D. Bandrauk, K. Vijayalakshmi and S. L. Chin, *J. Phys. B: At., Mol. Opt. Phys.*, 2000, **33**, 4615.
26 T. K. Kjeldsen, C. Z. Bisgaard, L. B. Madsen and H. Stapelfeldt, *Phys. Rev. A: At., Mol., Opt. Phys.*, 2005, **71**, 013418.
27 K. Kimura, S. Katsumata, Y. Achiba, T. Yamazaki and S. Iwata, *Handbook of HeI Photoelectron Spectra of Fundamental Organic Molecules*, Japan Scientific Societies Press, 1981.
28 B. Ruščić, L. Klasinc, A. Wolf and J. V. Knoop, *J. Phys. Chem.*, 1981, **85**, 1486.
29 A. G. Sage, T. A. Oliver, D. Murdock, M. B. Crow, G. A. Ritchie, J. N. Harvey and M. N. Ashfold, *Phys. Chem. Chem. Phys.*, 2011, **13**, 8075–8093.
30 S. Unny, Y. Du, L. Zhu, K. Truhins, R. J. Gordon, A. Sugita, M. Kawasaki, Y. Matsumi, R. Delmdahl, D. H. Parker and A. Berces, *J. Phys. Chem. A*, 2001, **105**, 2270.
31 M. Kadi, J. Davidsson, A. N. Tarnovsky, M. Rasmusson and E. Åkesson, *Chem. Phys. Lett.*, 2001, **350**, 93.
32 S.-H. Lee, K.-C. Tang, I.-C. Chen, M. Schmitt, J. P. Shaffer, T. Schultz, J. G. Underwood, M. Z. Zgierski and A. Stolow, *J. Phys. Chem. A*, 2002, **106**, 8979.
33 M. Rasmusson, R. Lindh, N. Lascoux, A. N. Tarnovsky, M. Kadi, O. Kühn, V. Sundström and E. Åkesson, *Chem. Phys. Lett.*, 2003, **367**, 759.
34 O. Anders Borg, D. Karlsson, M. Isomäki-Krondahl, J. Davidsson and S. Lunell, *Chem. Phys. Lett.*, 2008, **456**, 123.
35 M. N. R. Ashfold, B. Cronin, A. L. Devine, R. N. Dixon and M. G. D. Nix, *Science*, 2006, **312**, 1637.
36 A. L. Sobolewski, W. Domcke, C. Dedonder-Lardeux and C. Jouvet, *Phys. Chem. Chem. Phys.*, 2002, **4**, 1093.
37 T. G. Dietz, M. A. Duncan, M. G. Liverman and R. E. Smalley, *J. Chem. Phys.*, 1980, **73**, 4816.
38 C. W. Wilkerson, Jr and J. P. Reilly, *Anal. Chem.*, 1990, **62**, 1804.
39 P. Y. Cheng, D. Zhong and A. H. Zewail, *Chem. Phys. Lett.*, 1995, **237**, 399.
40 J. Matsumoto, C.-H. Lin and T. Imasaka, *Anal. Chem.*, 1997, **69**, 4524.
41 S. M. Hankin, D. M. Villeneuve, P. B. Corkum and D. M. Rayner, *Phys. Rev. Lett.*, 2000, **84**, 5082.
42 M. Lezius, V. Blanchet, M. Yu. Ivanov and A. Stolow, *J. Chem. Phys.*, 2002, **117**, 1575.
43 A. Abo-Riziq, L. Grace, E. Nir, M. Kabelac, P. Hobza and M. S. de Vries, *Proc. Natl. Acad. Sci. U. S. A.*, 2005, **102**, 20.
44 Y. Mairesse, J. Higuet, N. Dudovich, D. Shafir, B. Fabre, E. Mével, E. Constant, S. Patchkovskii, Z. Walters, M. Yu. Ivanov and O. Smirnova, *Phys. Rev. Lett.*, 2010, **104**, 213601.
45 A. Becker and F. H. M. Faisal, *Phys. Rev. A: At., Mol., Opt. Phys.*, 1999, **59**, R3182.
46 R. Wiehle and B. Witzel, *Phys. Rev. Lett.*, 2002, **89**, 223002.
47 R. Trebino, *Frequency-Resolved Optical Gating: the Measurement of Ultrashort Laser Pulses*, Kluwer Academic Publishers, 2002.